Electronic Supplementary Material (ESI) for Analyst.

Supplementary information

Quantitative analysis of binary and ternary organo-mineral solid dispersions by Raman spectroscopy for robotic planetary exploration missions on Mars

L. Demaret[1,2], I.B. Hutchinson[3], G. Eppe[1], C. Malherbe[1,2,3]

[1] Mass Spectrometry Laboratory, MolSys Research Unit, University of Liège, Liège, Belgium

[2] Early Life Traces & Evolution Laboratory, UR Astrobiology, University of Liège, Liège, Belgium

[3] Department of Physics and Astronomy, University of Leicester, Leicester, United Kingdom

Corresponding author: C. Malherbe - C.Malherbe@uliege.be

Table A: SEM micrographs of granular constituents making up dispersions evaluated by Raman spectroscopy.

Gypsum mineral matrix	Calcite mineral matrix	Organic analytes
Synthetic crystal	Synthetic crystals	Synthetic Cysteine
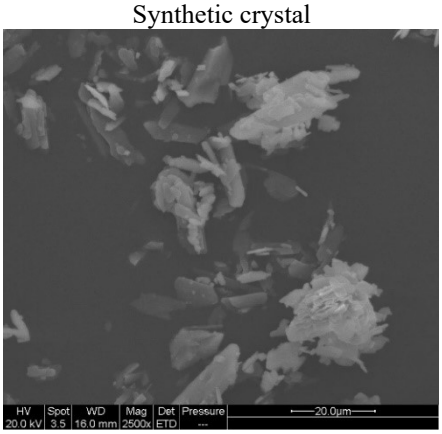	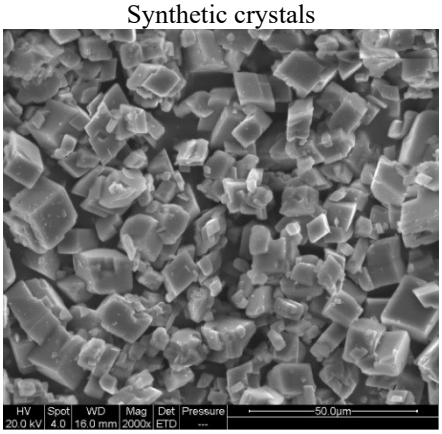	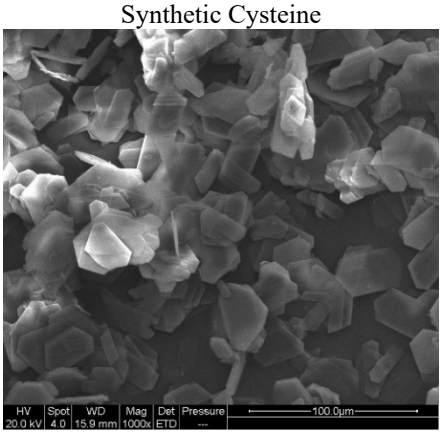
Mineral specimens (fraction <50µm)	Mineral specimens (fraction <50µm)	Synthetic Adenine
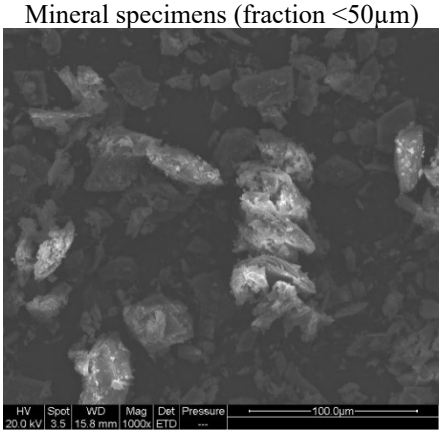	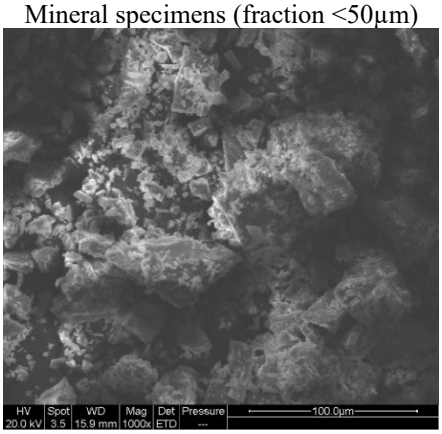	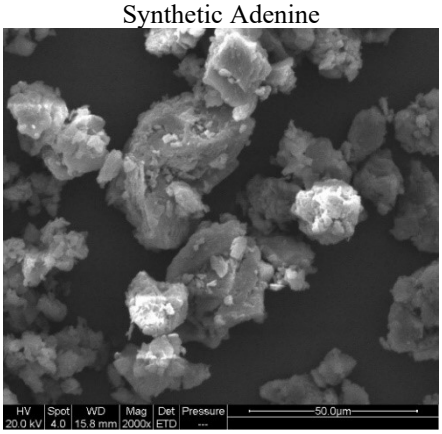
Mineral specimens (fraction: 50-100µm)	Mineral specimens (fraction: 50-100µm)	Synthetic Anthracene
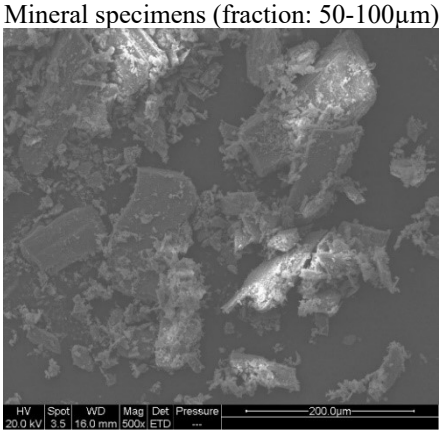	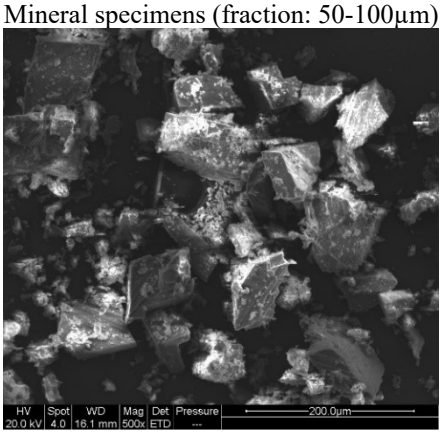	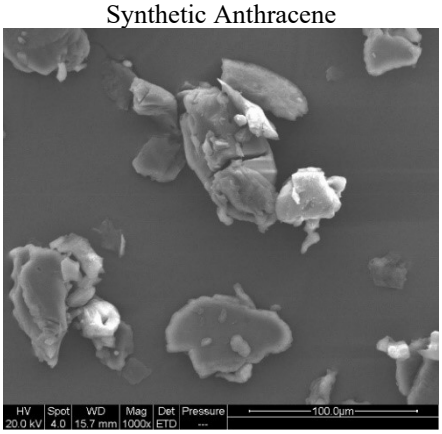
Mineral specimens (fraction >100µm)	Mineral specimens (fraction >100µm)	Synthetic Phthalic acid
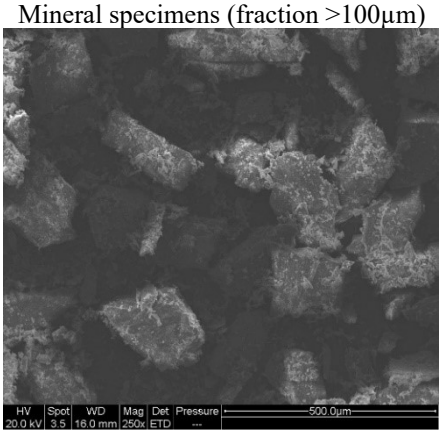	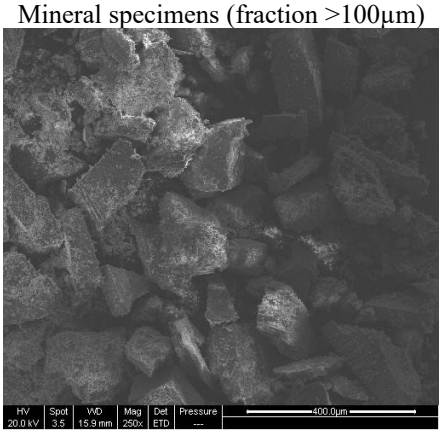	

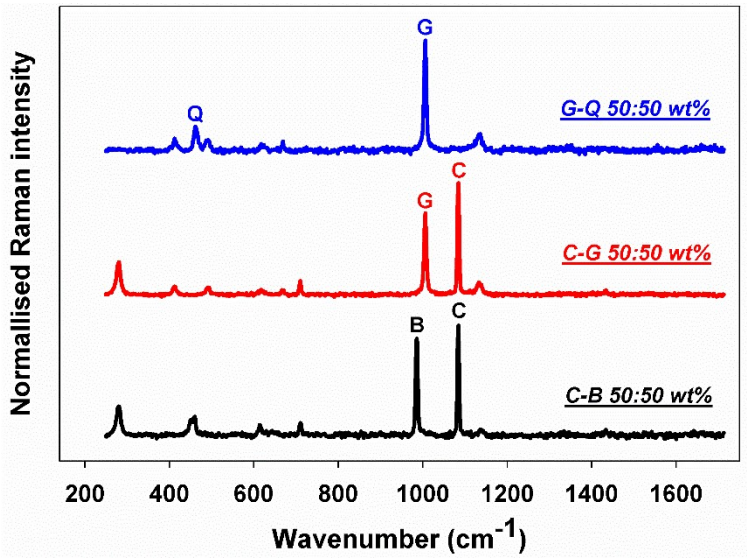

Figure S1: Typical Raman spectra from binary mineral mixtures (chemical standards) analysed using the Superhead Raman set-up. Baseline-corrected spectra from a mixture of calcite-baryte at 50:50 wt% (black colour), from a mixture of calcite-gypsum at 50:50 wt% (red colour) and from a mixture of gypsum-quartz at 50:50 wt% (blue colour). The main Raman band of each mineral phase is highlighted by its corresponding symbol. Abbreviations: B: baryte; C: calcite; G: gypsum; Q: quartz.

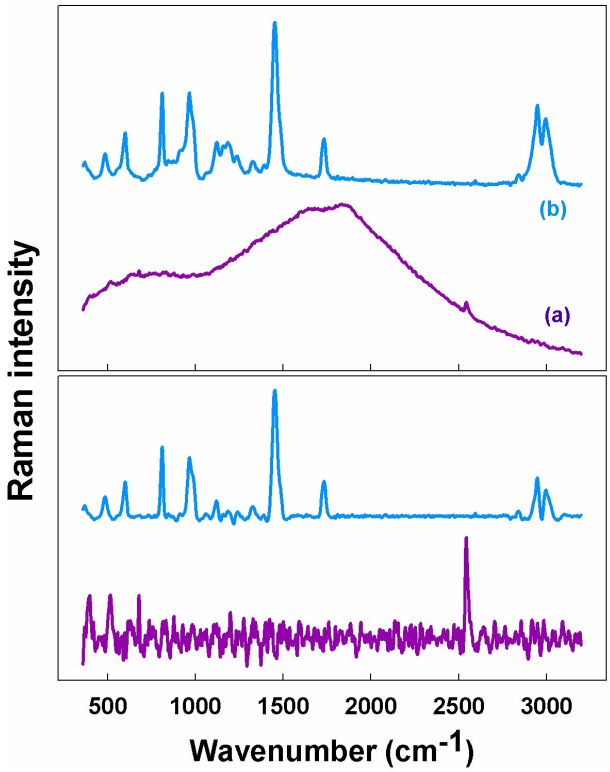

Figure S2: Typical Raman spectra obtained using the portable Raman spectrometer from (**a**) a dispersion of cysteine in clay at 18 wt% and; (**b**) a calibration standard of PMMA. Raw spectral profiles are presented in the upper window and the baseline corrected spectra in the lower window.

Table B: Summary of the data obtained using the Raman quantitative model for various dispersions of organics in mineral matrices. Reported concentrations, average intensities, standard deviations and relative standard deviations obtained from measurements with the portable instrument.

Type of dispersion	**Concentration** (wt%)	**Replicates - $I_{Norma\ (i=36)}$**			**Mean $I_{Norma\ (n=3)}$**	±	**SD**	**RSD** (%)
		(1)	**(2)**	**(3)**				
Cysteine in gypsum	10.05	12.75	13.47	12.95	13.1	±	0.4	3
	8.032	8.77	8.38	8.39	8.5	±	0.2	2
	6.032	7.46	7.68	5.59	7	±	1	14
	4.023	5.34	4.39	3.44	4	±	1	25
	2.014	1.88	1.73	2.01	1.9	±	0.1	5
Cysteine in calcite	10.00	11.85	11.36	12.21	11.8	±	0.4	3
	7.991	10.27	7.75	7.33	8	±	2	25
	5.596	6.62	5.66	4.66	6	±	1	17
	4.002	3.41	3.82	3.04	3.4	±	0.4	12
	2.002	2.29	2.54	2.47	2.4	±	0.1	4
Cysteine in clay	19.98	6.33	5.96	5.52	5.9	±	0.4	7
	17.99	4.37	6.09	5.55	5.3	±	0.9	17
	15.95	4.58	4.62	4.77	4.7	±	0.1	2
	13.94	4.04	4.34	4.54	4.3	±	0.2	5
	12.16	4.83	2.77	3.84	3.8	±	1	26
Adenine in gypsum	10.01	42.20	46.24	58.81	49	±	9	18
	8.000	34.28	27.98	47.14	40	±	10	25
	6.024	23.82	25.99	25.52	25	±	1	4
	3.978	14.17	20.88	19.12	18	±	4	22
	2.058	6.41	8.07	6.64	7.0	±	0.9	13
Phthalic acid in gypsum	12.07	6.88	7.91	6.84	7.2	±	0.6	8
	10.02	5.55	8.64	6.07	7	±	2	29
	8.012	5.93	6.51	4.97	5.8	±	0.8	14
	6.008	5.32	3.73	2.52	4	±	1	25
	4.006	1.87	1.81	4.04	3	±	1	33
Anthracene in gypsum	0.6552	9.29	9.96	9.64	9.6	±	0.3	3
	0.5460	7.49	5.63	7.98	7	±	1	14
	0.4536	7.76	6.00	5.59	6	±	1	17
	0.3528	5.25	4.95	2.64	4	±	1	25
Cysteine in gypsum-calcite	10.00	10.89	10.64	10.04	10.5	±	0.4	4
	8.00	8.78	8.27	8.53	8.5	±	0.3	4
	6.00	6.78	6.50	6.51	6.6	±	0.2	3
	4.00	4.02	4.14	3.77	4.0	±	0.2	5

Table C: Results from calculated intensity ratios ($I_{(n=3)}$) of mineral mixtures in various relative proportions (wt%). The data were obtained from dispersions of synthetic inorganic chemicals evaluated from grid-point scanning with the Superhead set-up.

Baryte – Calcite mixtures										
	φ_1 (B)	**φ_2** (C)	**φ_1** (B)	**φ_2** (C)	**φ_1** (B)	**φ_2** (C)	**φ_1** (B)	**φ_2** (C)	**φ_1** (B)	**φ_2** (C)
Proportion (wt%)	*20.10*	*79.90*	*40.00*	*60.00*	*50.00*	*50.00*	*59.98*	*40.02*	*79.90*	*20.10*
Intensity (Normalised)	17.82	82.18	38.92	61.08	49.09	50.91	59.16	40.84	79.13	20.87
SD	0.34	0.34	0.16	0.16	0.45	0.45	0.26	0.26	0.39	0.39
Intensity (F-corrected & normalised)	18.75	81.25	40.42	59.58	50.65	49.35	60.66	39.34	80.14	19.86
SD	0.35	0.35	0.17	0.17	0.45	0.45	0.25	0.25	0.38	0.38

Gypsum – Calcite mixtures										
	φ_1 (G)	**φ_2** (C)	**φ_1** (G)	**φ_2** (C)	**φ_1** (G)	**φ_2** (C)	**φ_1** (G)	**φ_2** (C)	**φ_1** (G)	**φ_2** (C)
Proportion (wt%)	*20.13*	*79.87*	*40.00*	*60.00*	*49.99*	*50.01*	*60.02*	*39.98*	*79.93*	*20.07*
Intensity (Normalised)	15.69	84.31	33.00	67.00	42.79	57.21	52.71	47.29	74.67	25.33
SD	0.21	0.21	0.61	0.61	0.21	0.21	0.50	0.50	0.32	0.32
Intensity (F-corrected & normalised)	20.05	79.95	39.91	60.09	50.21	49.79	60.04	39.96	79.90	20.10
SD	0.25	0.25	0.66	0.66	0.21	0.21	0.49	0.49	0.27	0.27

Quartz – Gypsum mixtures										
	φ_1 (Q)	**φ_2** (G)	**φ_1** (Q)	**φ_2** (G)	**φ_1** (Q)	**φ_2** (G)	**φ_1** (Q)	**φ_2** (G)	**φ_1** (Q)	**φ_2** (G)
Proportion (wt%)	*20.02*	*79.98*	*39.99*	*60.01*	*50.01*	*49.99*	*59.98*	*40.02*	*79.97*	*20.03*
Intensity (Normalised)	6.66	93.34	16.35	83.65	23.06	76.94	30.87	69.13	54.10	45.90
SD	0.11	0.11	0.28	0.28	0.57	0.57	0.63	0.63	0.31	0.31
Intensity (F-corrected & normalised)	19.49	80.51	39.85	60.15	50.42	49.58	60.22	39.78	80.00	20.00
SD	0.27	0.27	0.49	0.49	0.80	0.80	0.68	0.68	0.19	0.19

Study on the variability of Raman intensity for measurements obtained from a sample and between replicates.

The statistical data reported in the Table D from crushed gypsum and calcite spiked with cysteine described the variability between:

(a) the measurements at several locations along a grid-pattern on one given sample (intra-sample variability), and
(b) the measurements obtained for several replicates consisting in different aliquots of one concentration level (inter-sample variability).

Relative standard deviations (RSD) above 50% can be obtained for the intra-sample variability because the laser spot is often smaller than the grain of minerals interrogated in one location on the sample. Such local heterogeneities are inevitable with solid dispersions (in opposition to what is encountered with liquid solutions), yet controlled when applying a multi-spectra analytical procedure (here, the number of spectra averaged is i=36). Indeed, when datasets are replicated from various aliquots, the variability can drop below 25 % (RSD).

Table D: Statistical parameters (mean, SD, RSD) evaluated from the Raman intensities (i=36) of a grid-point mapping applied on a test portion of sample (intra-sample variability) and from replicated sets on various independent test portions of sample (inter-sample variability). The response from selected two types of dispersions (binary and ternary mixtures) is highlighted.

Type of dispersion		**Intra-sample variability**				**Inter-sample variability**						
						Replicates						
Binary mixture		**Mean**	**±**	**SD**	**RSD**	(1)	(2)	(3)	**Mean**	**±**	**SD**	**RSD**
Cys in gypsum	I_{Gypsum} (i=36)	10000	±	2000	20	10584	10122	9425	10000	±	600	6
at 6 wt%	$I_{Cysteine}$ (i=36)	700	±	300	43	748	730	515	700	±	100	14
	I_{Norma} (i=36)	8	±	4	50	7.46	7.68	5.59	7	±	1	14
Ternary mixture		**Mean**	**±**	**SD**	**RSD**	(1)	(2)	(3)	**Mean**	**±**	**SD**	**RSD**
Cys in C-G (50:50)	I_{Gypsum} (i=36)	1900	±	700	37	1932	1906	1946	1930	±	20	1
at 6 wt%	$I_{Calcite}$ (i=36)	2000	±	1000	50	2134	2261	2116	2170	±	80	4
	$I_{Cysteine}$ (i=36)	270	±	60	22	260	269	227	250	±	20	8
	I_{Norma} (i=36)	7	±	2	29	7.19	7.28	6.38	7	±	1	14

Mathematical developments for quantitative models of binary mineral mixtures: determination of $C_{\varphi 1}$ & $C_{\varphi 2}$

To quantify the proportion of two minerals φ_1 and φ_2 admixed into a solid dispersion, a set of equations must be employed in order to determine the concentrations $C_{\varphi 1}$ and $C_{\varphi 2}$ of each phase from their measured intensities $I_{\varphi 1}$ and $I_{\varphi 2}$, respectively.

First, the quantitative mathematical models that express the dependence of the Raman intensity for the concentration of a species correspond for the mineral phase φ_1 and φ_2 to the Eq. A.1(a) and Eq. A.1(b). When the two phases co-occur in a mixture, these two individual equations are combined according to the Eq. A2.

$$I_{\varphi 1} = r_{\varphi 1} C_{\varphi 1} \#(A.1a)$$

$$I_{\varphi 2} = r_{\varphi 2} C_{\varphi 2} \#(A.1b)$$

$$\frac{C_{\varphi 1}}{C_{\varphi 2}} = \frac{I_{\varphi 1} r_{\varphi 2}}{I_{\varphi 2} r_{\varphi 1}} \#(A.2)$$

For all binary mineral mixtures, the relative proportion of the two mineral phases admixed into a dispersion is always equal to 100% by weight (Eq. A.3). For various proportions tested, it was demonstrated that the ratio of apparent Raman scattering coefficients led to a constant value called the correction factor $F_{\varphi 2/\varphi 1}$, which is characteristic of a binary mineral system and is defined by the Eq. A.4, assuming φ_2 is always the phase with the larger apparent Raman scattering coefficient ($\boldsymbol{F_{\varphi 2/\varphi 1} > 1}$).

$$C_{\varphi 1} + C_{\varphi 2} = 100 \#(A.3)$$

$$F_{\varphi 2/\varphi 1} = \frac{r_{\varphi 2}}{r_{\varphi 1}} \#(A.4)$$

By substituting the Eq. A.4 into the Eq. A.2, the Eq. A.5 only has the concentrations and intensities as variables.

$$C_{\varphi 1} = \frac{I_{\varphi 1}}{I_{\varphi 2}} \cdot \frac{F_{\varphi 2}}{\varphi 1} \cdot C_{\varphi 2} \#(A.5)$$

An equation for determining $C_{\varphi 2}$ can be obtained by replacing Eq. A.5 into Eq. A.3:

$$\frac{I_{\varphi 1}}{I_{\varphi 2}} \cdot \frac{F_{\varphi 2}}{\varphi 1} \cdot C_{\varphi 2} + C_{\varphi 2} = 100 \#(A.6)$$

Finally, $C_{\varphi 1}$ is determined from the Eq. A.7:

$$C_{\varphi 1} = 100 - C_{\varphi 2} \#(A.7)$$

Mathematical developments for the corrected normalised intensities plotted for the graphs of binary mixture models.

The Figure S3 presents an example of calibration curves employed for the quantification of binary mineral mixtures, where the mineral phase φ_1 and φ_2 occur at various relative proportions by mass and account for a total of 100% (Eq. B.1). For such graphs, normalised intensities (e.g. $I_{norma\ \varphi1}$) are generally plotted as a function of the weight proportion (e.g. $C_{\varphi1}$) using an equation such as the Eq. B.2, assuming the sum of all intensities is set to 1.

$$C_{\varphi1} + C_{\varphi2} = 100\ \#(B.1)$$

$$I_{Norma\ (\varphi1)} = \frac{I_{\varphi1}}{I_{\varphi1} + I_{\varphi2}}\ \#(B.2)$$

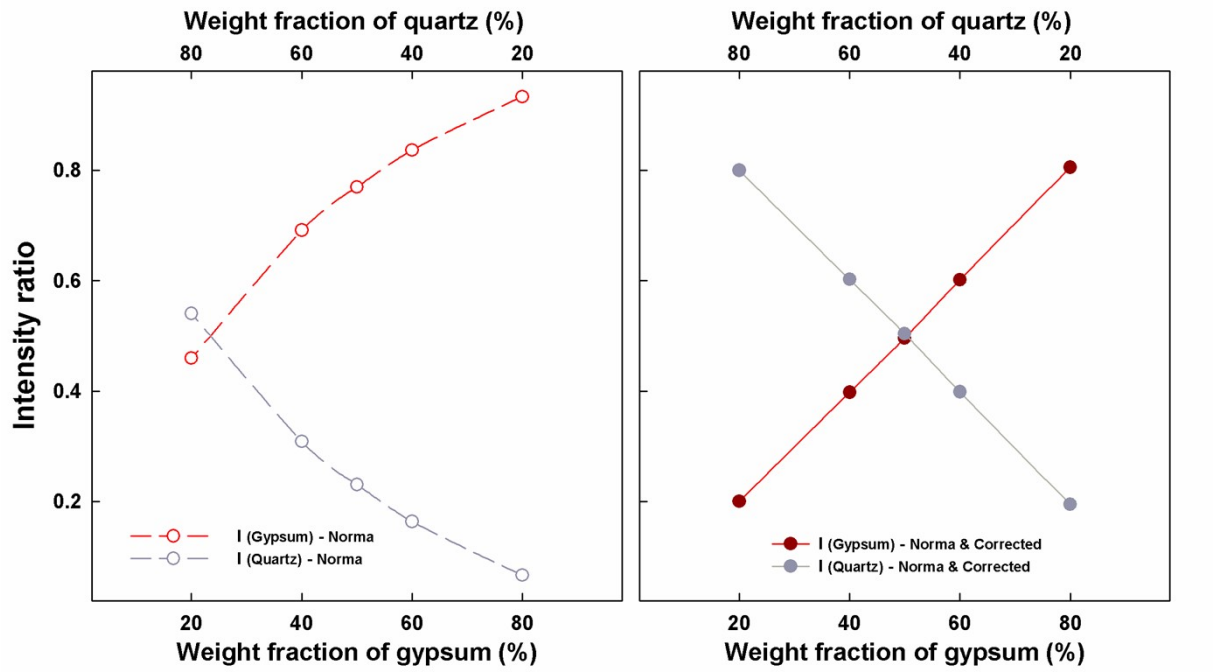

Figure S3: Calibration curves for binary mixtures of gypsum and quartz in varying weighed proportions (20:80 – 40:60 – 50:50 – 60:40 – 80:20) obtained with the Superhead set-up. Intensity ratio are expressed using the normalised intensities calculated based on the Eq. B.2 (left panel); and the normalised and corrected intensities based on the Eq. B.3 and Eq. B.4 (right panel).

It was demonstrated that the curves for the normalised intensities evolve linearly with the weight fraction when the mineral phases φ_1 and φ_2 have similar Raman scattering efficiencies (i.e. $\boldsymbol{F_{\varphi2/\varphi1}}$ 1), but diverge for minerals having different Raman scattering behaviours (Fig S3, left panel). Indeed, if the mineral phases φ_1 and φ_2 have identical responses, the normalised intensities, which are described by Eq. B.2 as an expression of molar fraction for intensities, are directly proportionally to the weighted mass fraction and lead to linear calibration curves.

Therefore, to establish the curves presented in the right panel of Fig S3, the normalised intensities must be corrected by expressing the response of the second mineral phase as if it involved the response of the

first mineral phase (i.e. identical responses from φ_1 and φ_2). Accordingly, for the mineral phase φ_1, we used the corrected normalised intensity $\mathbf{I'_{Norma\ (\varphi 1)}}$ presented in the Eq. B.3, where $I_{\varphi 2}$ is replaced by $I_{\varphi 1}^{*}$ (response from φ_2 as if it was consisting of φ_1). Re-expressing $I_{\varphi 2}$ as $I_{\varphi 1}$ can be done using the correction factor $\boldsymbol{F_{\varphi 2/\varphi 1}}$. The same reasoning applies for the mineral phase φ_2, from which the corrected normalised intensity $\mathbf{I'_{Norma\ (\varphi 2)}}$ is given by the Eq. B.4.

$$I'_{Norma\ (\varphi 1)} = \frac{I_{\varphi 1}}{I_{\varphi 1} + I_{\varphi 1}^{*}} \cdot (100) = \frac{I_{\varphi 1}}{I_{\varphi 1} + \frac{I_{\varphi 2}}{F_{\varphi 2/\varphi 1}}} \cdot (100) \#(B.3)$$

$$I'_{Norma\ (\varphi 2)} = \frac{I_{\varphi 2}}{I_{\varphi 2}^{*} + I_{\varphi 2}} \cdot (100) = \frac{I_{\varphi 2}}{I_{\varphi 1} \cdot F_{\varphi 2/\varphi 1} + I_{\varphi 2}} \cdot (100) \#(B.4)$$

The transformation from Eq. B.3 to Eq. B.4 comes as follow:

$$I'_{Norma\ (\varphi 1)} + I'_{Norma\ (\varphi 2)} = 1\ \#(B.4a)$$

$$I'_{Norma\ (\varphi 2)} = 1 - I'_{Norma\ (\varphi 1)} \#(B.4b)$$

$$I'_{Norma\ (\varphi 2)} = 1 - \frac{I_{\varphi 1}}{I_{\varphi 1} + \frac{I_{\varphi 2}}{F_{\varphi 2/\varphi 1}}} \#(B.4c)$$

$$I'_{Norma\ (\varphi 2)} = 1 - \frac{I_{\varphi 1} \cdot F_{\varphi 2/\varphi 1}}{I_{\varphi 1} \cdot F_{\varphi 2/\varphi 1} + I_{\varphi 2}} \#(B.4d)$$

$$I'_{Norma\ (\varphi 2)} = \frac{\left(I_{\varphi 1} \cdot F_{\varphi 2/\varphi 1} + I_{\varphi 2}\right) - I_{\varphi 1} \cdot F_{\varphi 2/\varphi 1}}{I_{\varphi 1} \cdot F_{\varphi 2/\varphi 1} + I_{\varphi 2}} \#(B.4e)$$

$$I'_{Norma\ (\varphi 2)} = \frac{I_{\varphi 2}}{I_{\varphi 1} \cdot F_{\varphi 2/\varphi 1} + I_{\varphi 2}} \#(B.4f)$$